Journal of Applied Mechanics Vol. 1 (August 1998) JSCE

Fracturing Response Simulation of FRP-Reinforced Concrete Beams by Mixed Finite Elements

Zhishen WU*, Jun YIN** and Toshihiro ASAKURA***

* Member Dr. of Eng., Asso. Prof., Dept. of Urban & Civil Eng. Ibaraki Univ. (Hitachi, 316-0033)

** Member MS, Dept. of Urban & Civil Eng. Ibaraki Univ. (Hitachi, 316-0033)

*** Member Dr. of Eng., Manager, Structure Tech. Development Div., Railway Tech. Research Inst. (Kokubunji,185-8540)

A numerical analysis has been conducted to simulate and evaluate the strengthening effects of concrete beams with externally bonded fiber-reinforced plastics (FRP) sheets. Mixed finite elements are used to model the displacement discontinuities both in plain concrete body and along FRP-concrete interface where debonding caused by shear stress usually takes place. From experimental results, several failure phenomena, including concrete shear failure, debonding along the FRP-concrete interface and FRP rupture, were observed. Through a parametric analysis on concrete tensile strength, bond strength of interfacial layer and thickness of FRP sheet, the numerical simulation has been conducted and the analysis results are compared with the experimental ones. Thus, the mixed finite element formulation is proved to be efficient in analysis of debonding propagation problems in FRP-reinforced concrete structures.

Keywords: *fiber-reinforced plastics(FRP), mixed finite element, debonding, fracture energy*

1. INTRODUCTION

Fiber reinforced composites are increasingly becoming important in the construction industry, with great potential in many areas. Fibers such as glass, carbon, and aramid can be introduced in a certain position, volume, and direction in the matrix to obtain maximum efficiency. The advantages of fiber reinforced plastics (FRP) are strength-to-weight ratio, corrosion resistance, electromagnetic neutrality, and greater efficiency in construction compared with the more conventional materials. With the FRP being used in a broad range of structural applications, a large number of experiments have been carried for the engineering designers to have a better understanding and to capture the characteristics of reinforced concrete by externally bonded FRP sheets (or plates), from which it is shown that global composite function was provided by the bond between the concrete and FRP, and significant improvement in performance could be archived in terms of ultimate load, crack control and stiffness. The fracture responses were observed in form of flexural cracking in concrete, debonding along the FRP-concrete interface and FRP rupture due to tension fracture.

To investigate the fracture mechanism of FRP-reinforced concrete structures, it is also necessary to perform computational simulations hand in hand with the experimental approach. However, the nonlinearity of such FRP reinforced concrete is still much restrained due to the complicate failure behaviors both in plain concrete body and the bonded zone which connects the concrete and FRP sheets. A conventionally used approach is the smeared crack model, which smears discontinuities, such as cracks, and treats them as continuum with a degrading constitutive relation between stress and strain on the integration points in an element. This approach can not trace quantitatively and essentially the displacement discontinuities that have been commonly observed in experiments. Thus, the direct implement of fracture behaviors on displacement discontinuous interface seems more rational to be adopted The main objective of this paper is to use the mixed finite element[1], which was proposed by the authors based on displacement discontinuity and concept of fracture energy on discontinuous interface for both mode I and II fractures, to simulate the crack and debonding propagations of both concrete and FRP-concrete interface. Especially, attention has been paid to the debonding failure behavior. Because the debonding is mainly caused by shear stress along the FRP-concrete interface of the beams, it is assumed that only along shear direction the displacement discontinuity takes place. Some initial study[2,5] has been

done to trace the debonding behavior in terms of linear fracture mechanics. According to the experimental observation[3], two of failure modes, the complete debonding and FRP rupture, are well performed by the numerical analyses. The fracture mechanism and FRP strengthening effects on concrete beams are discussed. It is also demonstrated that the mixed finite element and the proposed model for debonding are efficient for FRP reinforced concrete analyses.

2. MIXED FINITE ELEMENT FORMULATION[1]

2.1 Discontinuous Displacement Approximation

For a solid body with internal displacement discontinuity, the principle of virtual work can be extended and written as

$$\begin{aligned}&\int_{V^+}\delta\boldsymbol{\varepsilon}^T\boldsymbol{\sigma}\,dV+\int_{V^-}\delta\boldsymbol{\varepsilon}^T\boldsymbol{\sigma}\,dV\\&+\int_{S_i^+}\delta\mathbf{u}_i^{+T}\mathbf{r}_i^+dS+\int_{S_i^-}\delta\mathbf{u}_i^{-T}\mathbf{r}_i^-dS\\&-\int_{V^+}\delta\mathbf{u}^T\mathbf{f}\,dV-\int_{V^-}\delta\mathbf{u}^T\mathbf{f}\,dV\\&-\int_{S_p^+}\delta\mathbf{u}^T\mathbf{p}^+dS-\int_{S_p^-}\delta\mathbf{u}^T\mathbf{p}^-dS=0\end{aligned}\qquad(1)$$

Let V be the domain occupied by a body, and S be the boundary of the domain. The body is subjected to a body force field $\mathbf{f}$ in V, and prescribed external traction $\mathbf{p}$ on S. $\mathbf{u}$ is displacement vector, $\boldsymbol{\varepsilon}$ is strain vector, $\boldsymbol{\sigma}$ is stress vector. As shown in Fig. 1, interfaces S_i^+ and S_i^- ($S_i = S_i^+ \cup S_i^-$) are created by the internal discontinuities and subdivide the domain V into V^+ and V^- ($V = V^+ \cup V^-$), in which + and - refer to the positive and negative sides of the interface. On the discontinuous interface S_i,

$$\mathbf{u}_i^+ - \mathbf{u}_i^- = \mathbf{u}_i \qquad (2)$$

$$\mathbf{r}_i^+ = -\mathbf{r}_i^- = \mathbf{r}_i \qquad (3)$$

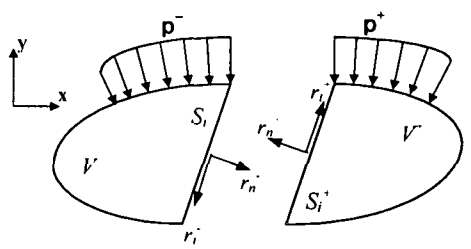

Fig. 1 Solid body with internal displacement discontinuity

$\mathbf{u}_i^+$ and $\mathbf{u}_i^-$ are displacements on the interfaces S_i^+ and S_i^- respectively. $\mathbf{r}_i^+$ and $\mathbf{r}_i^-$ denote the traction on the interfaces caused by relative displacement jump $\mathbf{u}_i$. The traction $\mathbf{r}_i$ is a function of the relative displacements $\mathbf{u}_i$.

Since all the following derivations are based on the displacement approximation, it is assumed that the displacement field with discontinuities is described as

$$\mathbf{u} \approx \mathbf{N}\bar{\mathbf{u}} + \mathbf{N}_d\bar{\mathbf{u}}_i \qquad (4)$$

in which $\mathbf{N}_d\bar{\mathbf{u}}_i$ is a discontinuous perturbation in the current displacement field approximation $\mathbf{N}\bar{\mathbf{u}}$. With the above displacement field approximation, the relative displacement field $\mathbf{u}_i$ along the internal interface is obtained as

$$\mathbf{u}_i = \mathbf{u}_i^+ - \mathbf{u}_i^- \approx (\mathbf{N}_d^+ - \mathbf{N}_d^-)\bar{\mathbf{u}}_i = \Delta\mathbf{N}_d\bar{\mathbf{u}}_i \qquad (5)$$

At the element level, it is assumed that a uniform deformation $\mathbf{u}_{i0}$ along the internal interface leads to a simple and efficient element formulation that the number of deformation modes consist with the dimension of the problem. In order to have a uniform deformation along the interface, the element displacement field is decomposed into a continuous part and a discontinuous part with a uniform discontinuity as

$$\mathbf{u} \approx \mathbf{N}\tilde{\mathbf{u}} + \mathbf{M}\mathbf{u}_{i0} \qquad (6)$$

in which $\tilde{\mathbf{u}}$ represents an imaginary nodal displacement of continuous part, while $\mathbf{u}_{i0}$ could be in form of

$$\mathbf{u}_{i0} = \left[u_{i0}^1 \quad \cdots \quad u_{i0}^{n_{sd}}\right]^T \qquad (7)$$

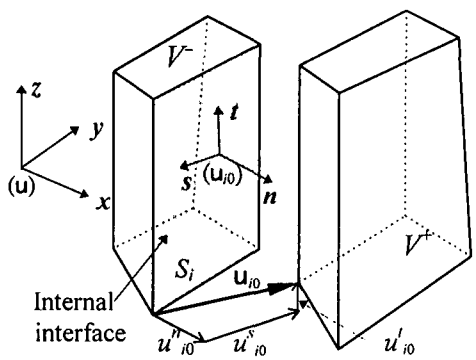

Fig. 2 Global and local systems of an interface for 3-D

that collects the magnitudes of n_{sd} uniform deformation modes of the internal discontinuities. $\mathbf{M} = M\,\mathbf{I}\,\mathbf{T}$, where $\mathbf{I}$ is a $n_{sd} \times n_{sd}$ identity matrix, $\mathbf{T}$ is a transformation matrix from local discontinuous interface to global co-ordinates. And M is a piecewise discontinuous function

$$M=\begin{cases}\alpha & in\ V^+\\ \alpha-1 & in\ V^-\end{cases} \qquad (8)$$

where $0\le \alpha \le 1$. The discontinuous function M is shown in Fig. 3 for two dimensional element.

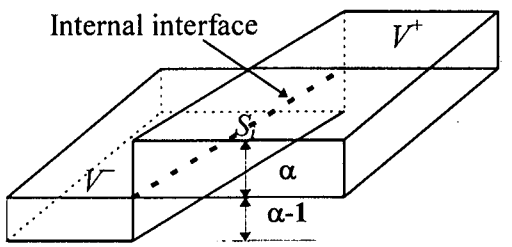

Fig. 3 Constant discontinuous function M in 2-D case

It can be seen that M reflects a unit jump across interface. With the displacement field approximation of (6)

$$\mathbf{u}_i = \mathbf{u}_i^+ - \mathbf{u}_i^- \approx (\mathbf{M}^+ - \mathbf{M}^-)\mathbf{u}_{i0} = \mathbf{u}_{i0} \qquad (9)$$

The displacement field of (6) should have a value equal to $\bar{\mathbf{u}}$ at the element nodes. From (9) and (6), this condition is enforced in form of

$$\bar{\mathbf{u}} = \tilde{\mathbf{u}} + \mathbf{P}\mathbf{u}_{i0} \qquad (10)$$

where $\mathbf{P}$ is a so-called piecewise matrix that redistributes the discontinuous displacements and transfers from the local discontinuous system, for three-dimensional, (n, t, s) to the global system (x, y, z)

$$\mathbf{P}=\left[M_1\mathbf{I}\quad M_2\mathbf{I}\quad \cdots\quad M_{n_{node}}\mathbf{I}\right]^T\mathbf{T} \qquad (11)$$

in which $M_i = M$ at node i. Substituting (9) into (6) leads to

$$\mathbf{u} \approx \mathbf{N}\bar{\mathbf{u}} + (\mathbf{M}-\mathbf{N}\mathbf{P})\,\mathbf{u}_{i0} \qquad (12)$$

Comparing with (4), the discontinuous shape function matrix $\mathbf{N}_d$ is obtained as

$$\mathbf{N}_d = \mathbf{M} - \mathbf{N}\mathbf{P} = N_d\,\mathbf{I} \qquad (13)$$

As we mentioned above, this formulation is based on the displacement field approximation. Therefore, enforcing the strain and stress fields calculations according to the continuous rules leads

$$\boldsymbol{\varepsilon} = \mathbf{B}\tilde{\mathbf{u}} \qquad \boldsymbol{\sigma} = \mathbf{D}\boldsymbol{\varepsilon} \qquad (14)$$

in which $\mathbf{B} = \mathbf{L}\mathbf{N}$ is the usual strain-displacement matrix, and $\mathbf{L}$ is the differential operator representing small deformation. $\mathbf{D}$ is the material tangent stiffness. Similarly, on the nonlinear interface, the constitutive relationship in a incremental form are expressed as

$$\Delta\mathbf{r}_i = \mathbf{D}_i\,\Delta\mathbf{u}_{i0} \qquad (15)$$

It is assumed that the nonlinear discontinuity is localized behavior only on the interface S_i and other parts are still in continuum using linear elastic relation. Therefore, the equation (1) can be written as

$$\begin{aligned}&\int_V \delta\boldsymbol{\varepsilon}^T\boldsymbol{\sigma}\,dV + \int_{S_i} \delta\mathbf{u}_i{}^T\mathbf{r}_i\,dS\\ &-\int_V \delta\mathbf{u}^T\mathbf{f}\,dV - \int_S \delta\mathbf{u}^T\mathbf{p}\,dS = 0\end{aligned} \qquad (16)$$

Neglecting the body force items and discretizing equation (16) in incremental form leads to

$$\begin{bmatrix}\mathbf{K}_{11} & \mathbf{K}_{12}\\ \mathbf{K}_{21} & \mathbf{K}_{22}+\mathbf{K}_{ii}\end{bmatrix}\begin{Bmatrix}\Delta\bar{\mathbf{u}}\\ \Delta\bar{\mathbf{u}}_i\end{Bmatrix} = \begin{Bmatrix}\Delta\mathbf{f}_1\\ \Delta\mathbf{f}_2\end{Bmatrix} \qquad (17)$$

where

$$\begin{aligned}\mathbf{K}_{11} &= \int_V \mathbf{B}^T\mathbf{D}\mathbf{B}\,dV \qquad \mathbf{K}_{12} = \int_V \mathbf{B}^T\mathbf{D}\mathbf{B}_i\,dV\\ \mathbf{K}_{21} &= \int_V \mathbf{B}_i{}^T\mathbf{D}\mathbf{B}\,dV \qquad \mathbf{K}_{22} = \int_V \mathbf{B}_i{}^T\mathbf{D}\mathbf{B}_i\,dV\end{aligned} \qquad (18)$$

in which $\mathbf{B}_i = -\mathbf{B}\mathbf{P}$. $\Delta\mathbf{f}_1$ and $\Delta\mathbf{f}_2$ are defined as follows:

$$\begin{aligned}\Delta\mathbf{f}_1 &= \int_S \mathbf{N}^T\Delta\mathbf{p}\,dS + \int_V \mathbf{N}^T\Delta\mathbf{f}\,dV\\ \Delta\mathbf{f}_2 &= \int_S \mathbf{N}_d^T\Delta\mathbf{p}\,dS + \int_V \mathbf{N}_d^T\Delta\mathbf{f}\,dV\end{aligned} \qquad (19)$$

By condensing out $\Delta\bar{\mathbf{u}}_i$ in (17), the final finite element equations are reached in a general form:

$$\mathbf{K}^*\Delta\bar{\mathbf{u}} = \Delta\mathbf{f}^* \qquad (20)$$

where

$$\mathbf{K}^* = \mathbf{K} - \mathbf{K}\mathbf{P}(\mathbf{P}^T\mathbf{K}\mathbf{P}+\mathbf{K}_{ii})^{-1}\mathbf{P}^T\mathbf{K} \qquad (20.a)$$

$$\Delta\mathbf{f}^* = \Delta\mathbf{f}_1 + \mathbf{K}\mathbf{P}(\mathbf{P}^T\mathbf{K}\mathbf{P}+\mathbf{K}_{ii})^{-1}\Delta\mathbf{f}_2 \qquad (20.b)$$

and $\mathbf{K} = \mathbf{K}_{11}$ is the stiffness matrix of an intact displacement-based continuous element.

Equation (20) is the final finite element equations by employing the mixed finite element, from which it can be

seen that its form is very similar to that of conventional finite element for continuum though additional discontinuous nodes are inserted in cracked elements at the beginning of formulation. Hence, this mixed finite element is easy to be implemented into general proposed FEM code without increasing the total degrees of freedom.

2.2 Fracture Modes in FRP-Reinforced Concrete Beams

The FRP-reinforced concrete beam with a notch at the bottom is made by bonding FRP sheets on its tension zone. The beam is simply supported and subjected to a concentrated load at mid-span on the top, as shown in Fig.4. From experiments, three kinds of failure modes, including shear failure in concrete, debonding at FRP-concrete interface and FRP rupture, were observed. To simulate structural response of the beam accurately, the fracture models corresponding to these failure behaviors are discussed as follows.

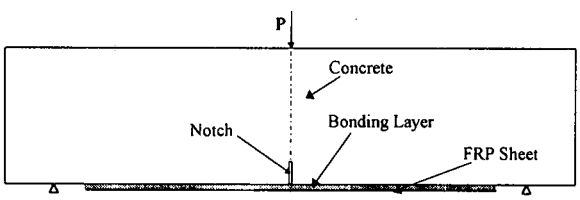

Fig.4 Loaded FRP reinforced concrete beam

(1) Mode I and Mode II Fractures in Concrete

Firstly, the fracture modes in plain concrete is discussed. Before crack initiation, concrete is regarded as linear elastic continuum. The material tangential stiffness matrix **D** for a plane stress element can be expressed

$$\mathbf{D}=\frac{E_c}{1-\upsilon^2}\begin{bmatrix}1 & \upsilon & 0\\ \upsilon & 1 & 0\\ 0 & 0 & \frac{1-\upsilon}{2}\end{bmatrix} \qquad (21)$$

where E_c is the Young's modulus of concrete. Once crack occurs, softening models on discontinuous interface are introduced. For simplicity, the constitutive matrix on the discontinuous interface $\mathbf{D}_i$ is specified that the off-diagonal terms are set zero since the coupling between the normal displacement and the shear displacement is considered to be less important in present study

$$\mathbf{D}_i=\begin{bmatrix}D^I & 0\\ 0 & D^{II}\ (or\ D_0^{II})\end{bmatrix} \qquad (22)$$

in which D^I is mode I tensile softening modulus and D^{II} is mode II shear softening modulus, D_0^{II} is the initial shear modulus before the mode II softening is entered. The areas contoured by the given stress-displacement diagrams of interface and axes equal to the values of fracture energy for mode I and mode II respectively, as shown in Fig.5. The present formulation assumes mode I fracture to be initiated firstly when principle stress reaches the tensile strength. Therefore, the shear stress across the crack is zero at the onset of cracking. That is why the shear softening diagram in Fig. 5 starts in the origin. Upon subsequent change of the principle stress axes a shear stress may develop across the interface until its maximum value τ whereafter the shear softening branch is started.

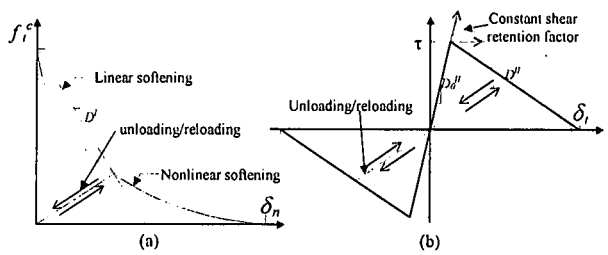

Fig. 5 (a) Mode I tensile softening
(b) Mode II shear softening

Furthermore, the unloading and reloading behaviors have been modeled by a secant path, which implies that on unloading the stress goes a linear line back to the origin. This procedure is applied to both mode I and mode II fracture. As mentioned previously, no coupling between mode I and mode II is considered. This makes it easy to trace the softening, unloading and reloading of mode I and mode II separately. For both modes, when unloading happens, the residual stresses at that point are stored as the beginning of the next softening procedure.

(2) Debonding along FRP-Concrete Interface

Debonding at the FRP-concrete interface where the concrete and FRP sheets are connected by adhesive, such as epoxy, is also an important failure phenomenon in FRP- reinforced concrete. From experiment observation, the debonding might propagate with the adhesive layer, through the concrete adjacent to the adhesive or along the

interface between the adhesive layer and FRP sheets. Because the interface layer mainly functions to transfer stress from concrete to FRP sheets by means of shearing, shear stress within the interface is much more dominant than tensile stress. Therefore, we assume that only shear modulus and bond shear strength have effects on those transferring interface elements. The material stiffness $\mathbf{D}_b$ can be written as

$$\mathbf{D}_b = \frac{E_b}{1-\upsilon^2}\begin{bmatrix} 0 & 0 & 0 \\ 0 & 0 & 0 \\ 0 & 0 & \frac{1-\upsilon}{2} \end{bmatrix} \qquad (23)$$

where E_b is the Young's modulus of FRP-concrete interface, ν is Poisson's ratio. In the numerical simulation of next section, debonding is regarded to occur in adhesive.

The shear stress in the interface is caused by the difference of deformation between concrete and FRP sheets. When its value exceeds the bond strength f^*_b that the interface can resist, the debonding occurs and subsequently propagates along the interface. Then, the shear stress will degrade and the constitutive relation of shear stress and bond-slip (slipping discontinuous displacement) in incremental form is given as, in Fig. 6. Therefore the constitutive equation on the debonding interface can be expressed

$$\Delta\tau = D_{bi} \cdot \Delta\delta_b \qquad (24)$$

The area between softening branch curve and axes is defined as fracture energy consumed for debonding propagation. The unloading and reloading procedures are considered in the way similar to that of concrete.

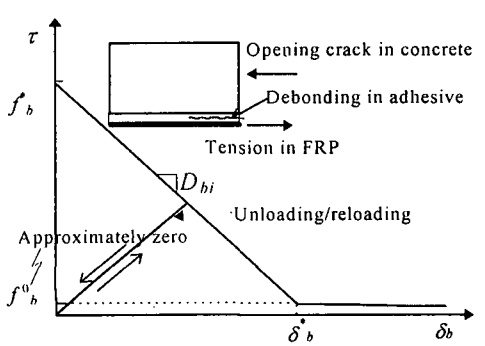

Fig.6 Softening branch of shear stress-relative displacement on debonding interface

(3) FRP Sheet Rupture

FRP sheet has been utilized as supplement of steel in reinforced concrete structures. Unlike steels, it can only resist tensile stress along its length and is assumed to be linear elastic until the ultimate tensile strength is reached. The material constitutive matrix for FRP elements is set as

$$\mathbf{D}_{FRP} = \frac{E_{FRP}}{1-\upsilon^2}\begin{bmatrix} 1 & 0 & 0 \\ 0 & 0 & 0 \\ 0 & 0 & 0 \end{bmatrix} \qquad (25)$$

where E_{FRP} is the Young's modulus of FRP sheet. The shear stiffness and tangent stiffness normal to the tension direction are ignored since they are less important than tension. If rupture happens, it follows a sudden drop of resistance to zero, as shown in Fig. 7

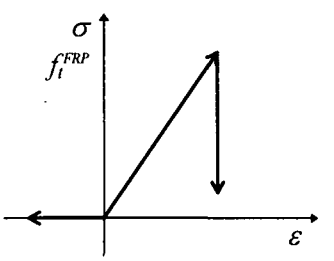

Fig.7 FRP stress-strain relation

Because the rupture, which may take place at any point in FRP sheets, predicts the final collapse of the whole reinforced concrete beam, numerical analysis will stop when the rupture is checked.

3. NUMERICAL SIMULATIONS

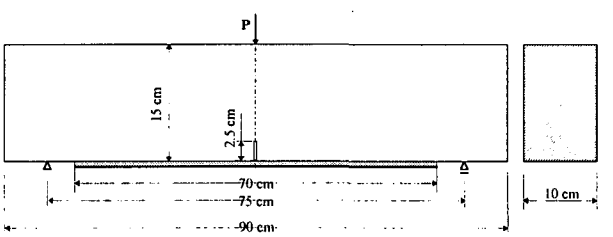

Fig.8 Details of FRP reinforced concrete beam

Based on the experimental data, a plain concrete beam with an initial notch at the mid-span is strengthened with adhered FRP sheets on the bottom face. The loading case and size of the beam is shown in Fig. 8.

In analysis procedure, only half of the beam is discretized by four-node plane stress finite elements for concrete, bonded zone and FRP sheets, in Fig.9. Four

point Gaussian integration is used in concrete elements, while reduced integration(1 point) is adopted for bonded transferring elements and FRP elements because their width are much thinner than the length.

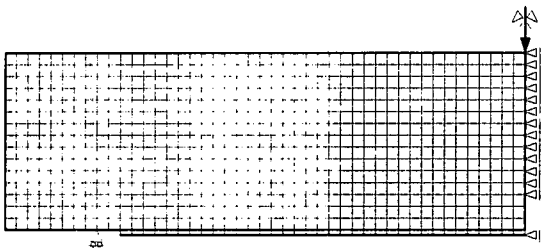

Fig.9 Finite element discretization

In this study, the strengthening effects and failure behavior will be discussed in three aspects as to the experiments: 1) in different concrete strength, 2) in different bonded strength of adhesive and 3) in different quantity of FRP sheets. Therefore, the numerical analyses are also conducted in these three aspects and comparison with experimental results are shown in the figures. The material properties and some simulation parameters are listed in Table.1 and Table 2 respectively

Table.1 Material properties

Concrete	Young's modulus (kgf/cm^2)	200,000~400,000
	Poisson ration	0.16
	Tensile strength (kgf/cm^2)	20.0~35.0
FRP sheets	Young's modulus (kgf/cm^2)	2,300,000
	Poisson ration	0.3
	Tensile strength (kgf/cm^2)	20,000
Adhesive	Young's Modulus (kgf/cm^2)	40,000
	Poisson ration	0.3

Table.2 Simulation parameters

Concrete	Fracture energy (kgf/cm)	0.15
Adhesive	Bond strength (kgf/cm^2)	5.0~35.0
	Bond slip (μm)	20

3.1 Effects of Concrete Tensile Strength

In the experiments, the concrete strength is specified by the compressive strength. However, to use the mixed finite element which checks the crack by tensile strength, the equivalent tensile strength is conversed from compressive one. In addition, the values of concrete Young's modulus are also varied correspondingly. In our analyses, three values of concrete tensile strength are selected as 20.0kgf/cm^2, 27.15kgf/cm^2 and 33.94kgf/cm^2 with their Young's modulus 278,000kgf/cm^2, 325,000kgf/cm^2 and 364,000kgf/cm^2 respectively. Since it is assumed that the concrete beam is well-bonded with the FRP sheets (thickness=0.1cm), a high bond strength of adhesive is used as 35kgf/cm^2.

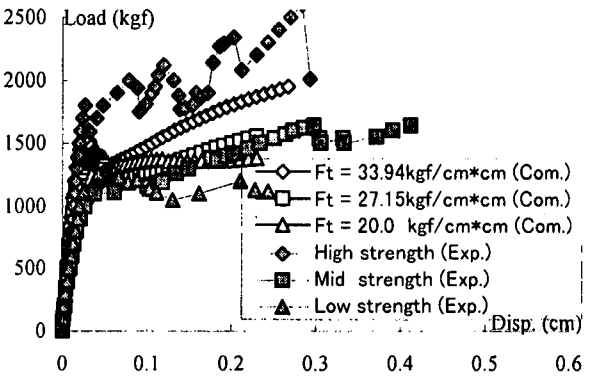

Fig. 10 Effects of concrete tensile strength

The computational (Com.) and experimental (Exp.) results of load-mid span deflection curve are shown in Fig.10. It can be seen that the analytical results approximately reflect the real responses in experiments in cases of different concrete strengths. Compared between these cases, it is found that the high strength concrete can bear higher load because the higher strength concrete with larger value of young's modulus makes stress in concrete increase more rapidly so that the tensile stress in FRP sheets also increase very soon to resist the external load. A softening behavior after crack loading is observed for those high strength concrete while the low one has no such a response. According to the numerical simulation, this can be explained that because the fracture energy is assumed to be same for the different strength concrete beams the softening tangential modulus is larger to high tensile strength concrete than the low one so that it follows a quick stress degradation right after that. Immediately, it rises up, where FRP sheets start to bear the load. Due to high bond strength of the interface, the debonding is not obvious. But it is found that the tensile stress in FRP sheets of high concrete strength beam is larger than that in low strength ones. For example, at the same deflection with Disp = 0.23cm in Fig.10, the tensile stresses of FRP sheets in three cases are 15,400kgf/cm^2, 13,300kgf/cm^2 and 10,600kgf/cm^2 from the high to the low concrete strength beam. It may be predicted that the final failure mode will be ended with FRP rupture occasionally in high concrete strength beam even though the debonding failure occurs in same concrete beam with

low strength concrete if FRP is bonded well enough on the concrete body.

3.2 Effects of Bond Strength of Adhesive

As observed in experiments, the debonding is a very important failure mode in FRP-reinforced concrete beam. It is considered to be effected by bonding behavior along FRP-concrete interface. On the other hand, the bond strength might be varied due to different degrees of bond imperfection or different construction conditions. To model this, the cases with different values of bond strength, which have the same concrete tensile strength 27.15kgf/cm^2 and thickness of FRP sheet 0.1cm, are tested. Table.3 lists three cases we have computed.

Table 3 Different bonded strengths

Bond Strength f_b^* (kgf/cm^2)	Fracture Energy G_b (kgf/cm)	Bond-slip δ_b^* (μm)
5.0	0.005	20
15.0	0.015	20
35.0	0.035	20

As discussed in section 2.2, the softening branch of shear stress-bond slip is given by means of fracture energy. However, the value of interfacial fracture energy hasn't been measured through experimental approaches. But the bond slip was really measured with average length about 20μm[4]. Hence, by giving different bond strengths, the corresponding fracture energies can be obtained.

The comparison of different bond strengths in Fig.11 shows that the case with well-bonded condition can bear higher and more durable load capacity.

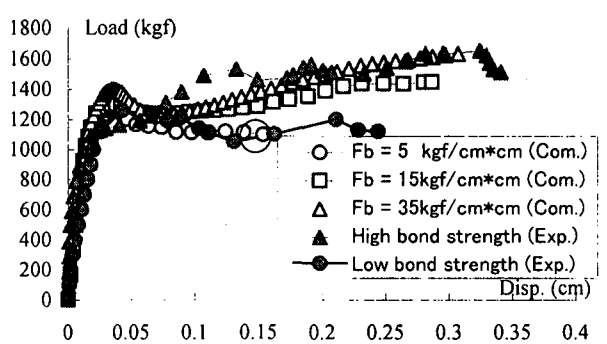

Fig. 11 Effects of bond strength of adhesive

For the bond strength of 35kgf/cm^2, only in one element in the middle of bottom the debonding happens; for 15kgf/cm^2 case, the debonding develops 12 elements along the bonded interface; while for 5kgf/cm^2 case, debonding occurs in all of 35 adhesive elements in the order from the middle to the edge, thus causes the final debonding failure of the whole reinforce concrete beam. The same results are observed in experiments: the debonding occurs quickly and propagates easily in low bond strength case so as to lead debonding failure finally, while the well-bonded beam can hold higher load with less debonding. The circle mark at the end of curve f_b=5kgf/cm^2 (Com.) in Fig.11 indicates the final debonding failure point.

When bonded strength is selected 35kgf/cm^2, since there is almost no debonding development along the FRP-concrete interface it can be regarded well-bonded with such a bond strength if the debonding propagate within the adhesive layer. On the other hand, if the well-bonded condition is assumed, the value of fracture energy of adhesive in shearing can be approximately identified by the measured bond slip and bond strength from the following equation

$$G_b \approx 1/2\ \delta_b \bullet f_b \qquad (26)$$

The crack patterns in these three cases also reflect apparent difference, in Fig. 12. It can be seen that in case of low bond strength, Fig.12(a), cracks in concrete body are mainly localized in the middle of the beam due to the quick debonding behavior of adhesive. On the contrary, in Fig.12(c), much more cracks occur, which are distributed in a triangle zone. It can be explained that the well-bonded conditions transfer the stress between FRP and concrete, and restrain the deformation of concrete.

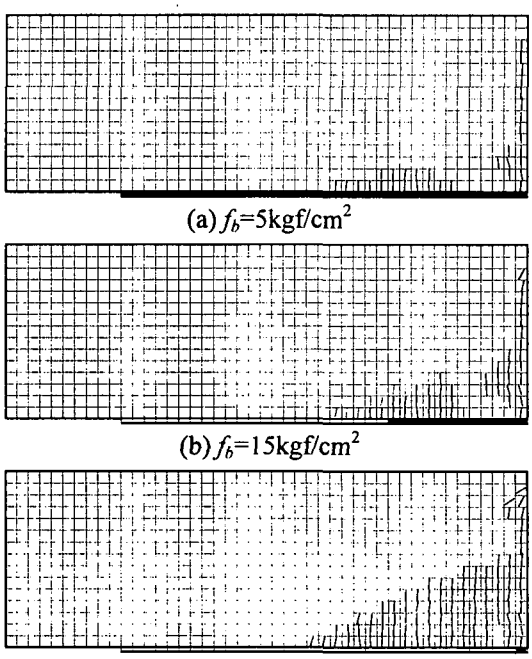

(a) f_b=5kgf/cm^2

(b) f_b=15kgf/cm^2

(c) f_b=35kgf/cm^2

Fig. 12 Crack patterns and debonding propagation

3.3 Effects of FRP Sheets Thickness

Two FRP-reinforced concrete beams were analyzed with same concrete tensile strength 27.15kgf/cm^2 and bond strength 15kgf/cm^2, the difference is that one beam is reinforced with one layer of FRP sheets with thickness 0.1cm and the another beam is reinforced with two layers of FRP sheets with thickness 0.2cm. The difference of strengthening effects are shown in Fig.13.

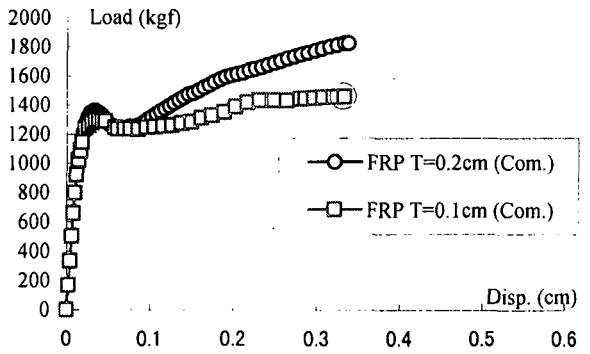

Fig.13 Effects of FRP sheets thickness

From the computational results, it can be seen that, for the beam with thin FRP sheet, the tensile stress increases rapidly because of small intersection area, but the structural load resistance is relatively low. It finally follows FRP rupture failure at the circle mark in Fig.14 where the stress exceeds the given FRP sheet tensile strength f_{FRP}=20,000kgf/cm^2. The FRP rupture is also found in thin FRP concrete beam in experiments. On the contrary, the thick FRP sheet beam can bear higher load though the tensile stress (only 12,000kgf/cm^2 at the last step) is not as high as that of the thin one. But more debonding elements have been found in the thick one. Until the end of analysis, there have been 20 elements in which debonding takes place in the thick FRP sheet beam while the thin one has 13 debonding elements. This can be explained by such a fact that the sufficient FRP sheets naturally increase the beam's stiffness and load capacity. However, the more FRP sheets are used, there is more remarkable relative deformation between the concrete and FRP sheets. That will lead to increase of shear stress in adhesive layer and thereafter likely debonding propagation. It can be predicted that a concrete beam with too thicker FRP-sheets will eventually follows debonding failure even though the sheet tensile stress may be much lower than its tensile strength. In this point of view, how to rationally design the quantity of FRP sheets used to strengthen concrete beam is still a topic to be explored.

4. CONCLUSION

Based on the fracture response simulation by the mixed finite elements embedded with displacement discontinuity, the proposed constitutive models is capable of predicting the crack and debonding propagation in concrete and along the FRP-concrete interface. In addition, the strengthening effects and failure mechanism have been discussed and identified by varying the material parameters, such as concrete strength, bond strength of adhesive and thickness of FRP sheets, and corresponding experimental results are compared. There are several conclusions obtained from analysis study:

1. The introduction of softening models with concept of fracture energy is acceptable, for both the concrete crack and debonding interface. It is necessary to be used in simulating these kinds of displacement discontinuities and their propagations with brittle fractures.

2. The dominant debonding behavior seriously reduces the structural load capacity of FRP reinforced concrete beams. It results from either difference constructional conditions or irrational strengthening design.

3. The design approach should be crystallized by interpreting some major modes of failure effected by relative parameters, which will be very instructive to the strengthening method in engineering applications.

REFERENCES

[1] Z.S. Wu, et.al, : Development of mixed finite element method for composite discontinuous analysis, J. Struct. Mech. & Earthquake Eng., JSCE, 1998.7. (to be appeared)

[2] Z.S. Wu, et.al, : Interface crack propagation in FRP strengthened concrete structure, Proceedings of 3rd Int. Symp. FRPRCS, Vol.1 pp.319-326, 1997.10.

[3] Z.S. Wu, et.al, : Experimental study on failure modes of FRP reinforced concrete beams (in Japanese), Proc. of 53th Annual Conf. of the JSCE, Vol.5, 1998.9. (to be appeared)

[4] A. Sharif, et.al, : Strengthening of initially loaded reinforced concrete beams using FRP plates, ACI Stuct. J, Vol.91, No.2, pp.160-168, 1991

[5] H. Yoshikawa and Z.S. Wu, : Fracture energy approach for predicting fracture response of RC tensile members strengthened with CFRP sheets, J. Struc. Eng. Vol.43A, 1997.

(Received April 24, 1998)